Science Arts & Métiers (SAM)
is an open access repository that collects the work of Arts et Métiers Institute of Technology researchers and makes it freely available over the web where possible.

This is an author-deposited version published in: https://sam.ensam.eu
Handle ID: .http://hdl.handle.net/10985/8058

To cite this version :

Sylvain RIVIERE, Sedigheh FARZANEH, Abbas TCHARKHTCHI, Farid BAKIR, Sofiane KHELLADI - Simulation of Polymer Flow Using Smoothed Particle Hydrodynamics Method - Polymer Engineering and Science - Vol. 53, n°12, p.2509-2518 - 2013

Any correspondence concerning this service should be sent to the repository Administrator : scienceouverte@ensam.eu

Simulation of Polymer Flow Using Smoothed Particle Hydrodynamics Method

S. Riviere,[1] S. Khelladi,[2] S. Farzaneh,[1] F. Bakir,[2] A. Tcharkhtchi[1]
[1] *PIMM laboratory, Arts et Métiers ParisTech, CNRS-UMR 8006, 151 Bd de l'hôpital 75013 Paris, France*

[2] *DynFluid Laboratory, Arts et Métiers ParisTech, 151 Bd de l'hôpital 75013 Paris, France*

Reactive rotational molding (RRM) is a process to manufacture hollow plastic articles. Comparing to rotational molding of thermoplastics, it decreases the process cycle time due to the reactivity of the system. However, the number of influent parameters is relatively high and optimization of the process is complex. During RRM, the viscosity is one of the key parameters and varies according to the polymer molecular weight due to chemical reactions. Simulation is a way to optimize this process. Prediction of the reactive flow is of great interest to optimize process conditions and wall thickness distribution of the molded part. We developed a solver based on smoothed particle hydrodynamics method. This Lagrangian meshfree method is well adapted to simulate free surface flows like those occurring in RRM. First, we validated the code comparing the simulation results to analytical Couette flow solution and experimental measurements of dam break problem. Then, we performed two-dimensional (2D) and 3D simulations to observe the influence of the change of viscosity on the flow, due to the chemical reactions. Adhesion of the polymer on the mold surface is modeled by new boundary conditions. **POLYM. ENG. SCI., 53:2509–2518, 2013.** **© 2013 Society of Plastics Engineers**

INTRODUCTION

Rotational molding is a process for manufacturing the hollow plastic parts from few centimeter to several meters [1, 2]. The main advantages of this method are no residual stresses in final parts, no weld line, and no heterogeneity of material behavior compared to other polymer processes such as injection molding or blowing extrusion. The mains weaknesses are the time to heat and melt the polymer powders and the time to cool and solidify the polymer. Consequently, the cycle time to produce a plastic part is long (0.5–1 h), depending on the dimensions of the part. Moreover, the range of polymer used is limited because, a low polymer melt viscosity and a high thermal stability are required. Nowadays, rotational molding of thermoplastics is widely used in industry; nevertheless, there are only few applications for reactive materials due to the complexity of the polymer transformation. The first work [3, 4] carried out in this field outlined these problems, partly because various states of flow occur in the mold according to the variation of viscosity. Reactive rotational molding (RRM) has several advantages compare to traditional rotomolding of thermoplastic powders: process cycle time is shorter, raw material is less expensive because polymerization occurs during processing, and high-performance polymers may be used such as thermosets (polyester [3], polyepoxy [5], and polyurethane [6, 7]) and thermoplastic (polyamide 6 [4, 8]) or blends (polyepoxy/poly(methyl methacrylate) [9]).

However, implementation of RRM is complex because of chemical reactions. Figure 1 shows the variation of viscosity related to the rheology evolution during polymerization. According to the conversion ratio, the viscosity increases and we can distinguish several hydrodynamic regimes. In the early step of the chemical reactions, the viscosity is low and the material cannot adhere to the mold surface ("pool"). At that point, the viscosity begins to increase and the material starts to adhere but due to gravity, it falls down, this is the cascading flow. Then, we can observe the rimming flow where the material is well distributed on the mold surface but a wave phenomenon is still occurring on the fluid surface. Finally, we can observe the solid rotation; this is the desired flow where the fluid is uniformly distributed on the internal mold surface. This flow must appear before the gel point of the material (Fig. 1c) where an infinite network is formed. Over this point, the material becomes stiff and there is no more flow. The chemical reactions are not completed but the part can be removed from the mold for the postcuring process. It is important to notice that these different kinds of flows are dependent on the viscosity and the rotational speed. Here, we can clearly see the importance of the

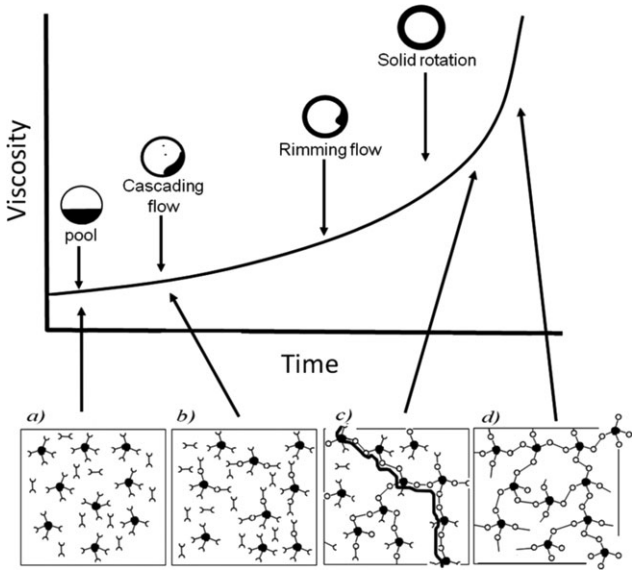

FIG. 1. Variation of viscosity and hydrodynamic regimes according to the conversion ratio.

simulation to predict the flow according to the mold geometry, the rotational speed of both axes, and the mold temperature that influences the reaction rate.

Until now, optimization of RRM is mainly based on the characterization of the reactive materials. From the thermal and the rheological analysis, the vitrification and the gelation are studied and the time–temperature transformation diagram [10–12] is drawn. This method is commonly used to determine the best process parameters and to predict the cycle time for thermosetting processes. Isoviscosity curves can be added to this diagram; however, it does not allow a good prediction of the flow for a given viscosity. Throne and Gianchandani [3] were the first to observe the different flows occurring during RRM. They described the above mentioned hydrodynamic regimes but it does not allow a good prediction of the flow for a complex mold geometry rotating around two perpendicular axes.

The first simulations carried out in this field used the volume of fluid method with a commercial software [13, 14]. These first simulations showed the influence of parameters, such as the rotation speed, the amount and the viscosity of the polymer, on the cycle time. However, the results were not good enough for a realistic prediction of the material flow, mainly because of the free surface representation and the absence of rheokinetical models [15, 16] to describe the evolution of viscosity according to reaction rate. Mounif [14] started to develop a solver based on smoothed particle hydrodynamics (SPH) method to simulate RRM. This meshfree particle method is particularly suited to simulate free surface flows such those occurring during RRM. SPH method was established in 1977 by Lucy [17], Gingold and Monaghan [18] to the field of astrophysics. Since then, this method was successfully applied to others scientific domains and particularly to fluid mechanics [19–22]. SPH method is already used to model material processing, notably metal forming [23, 24] and injection molding [25]. Since Mounif's work we improved the initial solver to be able to simulate two-dimensional (2D) and 3D flows. The reactive material used in the simulations is a polyurethane. To estimate the variation of viscosity according to the chemical reactions, we added a rheokinetical model [26] based on the experimental results and we implemented a new type of boundary condition to model the adhesion of the reactive fluid on the mold surface.

METHOD

To simulate the polymer flow during RRM, we applied SPH method. In pregel phase, where the viscosity is low, the fluid flow is characterized by a free surface flow with the competition of two main forces: gravity and viscosity. The fluid is modeled as an incompressible viscous Newtonian fluid because rotational speed is low (1–10 rpm) and shear force is negligible. Here, we only present the basics of SPH method, for details and references see the reviews by Monaghan [27, 28] and the book written by Liu and Liu [29].

Principles

In SPH method, material is represented by N particles of masse m_i, velocity v_i and others hydrodynamics properties such as pressure P_i, temperature T_i, viscosity n_i, etc. Particles sizes can vary from few micrometers to thousands of kilometers depending of the field of study [27, 29]. In SPH, the fundamental principle is to approximate any function A(r) by:

$$A(r) = \int A(r')W(r - r', h)dr' \tag{1}$$

where h is called the smoothing length and $W(r \quad r',h)$ is the weighting or kernel function. This approximation in discrete notation leads to the following approximation of the function at a particle a:

$$A(r) = \sum_b \frac{m_b}{\rho_b} A_b W_{ab} \tag{2}$$

where the summation is over all the particles within the region of compact support of the kernel function. m_b and ρ_b are, respectively, the mass and the density of particle b.

Smoothing Functions

The performance of an SPH simulation is closely dependant on the choice of the weighting function or smoothing kernel. They should satisfy several conditions such as positivity, compact support, and normalization. Furthermore, W_{ab} must decreases monotonously with the

increase in the distance from particle a and behaves like a delta function as the smoothing length, h tends to zero [29]. Kernels depend on the smoothing length and the nondimensional distance between particles given by $q = r/h$, r being the distance between particle a and b. The smoothing length or influence domain h, controls the size of the area around particle a where the particles b contribute to calculate properties of particles a. In our simulation we chose the cubic spline function which is widely used in the SPH literature.

$$W(r.h) = \alpha_D \begin{cases} 1 - \frac{3}{2}q^2 + \frac{3}{4}q^2 & 0 \leqslant q \leqslant 1 \\ \frac{1}{4}(2-q)^2 & 1 \leqslant q \leqslant 2 \\ 0 & q \geqslant 2 \end{cases} \quad (3)$$

where α_D is $\frac{10}{7\pi h^2}$ in 2D and $\frac{1}{\pi h^3}$ in 3D.

Continuity Equation

The changes in the fluid density are calculated according to the following equation:

$$\frac{d\rho_a}{dt} = \sum_b m_b(\vec{v}_a - \vec{v}_b)\vec{\nabla}W_{ab} \quad (4)$$

where ρ_a is the density of particle a, with velocity v_a and m_b is the mass of particle b. This equation is frequently used in the case of slightly compressible flow. This form which is Galilean invariant has good numerical conservation properties and is not affected by free surfaces or density discontinuities [23]. It is important to use this form of continuity equation for predicting the free surface flows such as those occurring in RRM.

Momentum Equation

The momentum conservation equation in a continuum field is:

$$\frac{d\vec{v}}{dt} = -\frac{1}{\rho}\vec{\nabla}p + \vec{g} + \vec{\Theta} \quad (5)$$

where Θ refers to the diffusion terms. Different approaches, based on various existing formulations of the diffusive terms can be considered in the SPH method to describe momentum equation. Most of implementations of SPH employ an artificial viscosity like those developed by Monaghan [27] or Cleary [30]. In these simulations we used the momentum equation developed by Morris et al. [21]:

$$\frac{d\vec{v_a}}{dt} = -\sum m_b\left(\frac{P_a}{\rho_a^2} + \frac{P_b}{\rho_b^2}\right)\vec{\nabla}W_{ab} + \sum \frac{m_b(\eta_a + \eta_b)v_{ab}}{\rho_a\rho_b}\left(\frac{1}{r_{ab}}\frac{\partial W_{ab}}{\partial r_a}\right) + \vec{g} \quad (6)$$

P_a, P_b and η_a, η_b are, respectively, the pressure and the viscosity of particles a and b. In this formulation, each particle has its own viscosity which can vary in time and that is interesting to introduce the rheokinetical model of the reactive material where the viscosity evolves according to the conversion ratio. Moreover this equation utilizes the dynamic viscosity and allows the use of high viscosity in the same scale as the viscosity of the gel point of the reactive material.

Equation of State

The fluid in SPH method formalism is treated as a weakly compressible material. This hypothesis facilitates the use of an equation of state to determine the fluid pressure, which is much faster than solving an equation such as the Poisson's equation. The equation of state, giving a relationship between particle density and fluid pressure is

$$P = P_0\left[\left(\frac{\rho}{\rho_0}\right)^\gamma - 1\right] \quad (7)$$

where P_0 is the magnitude of the pressure and ρ_0 is the reference density. P_0 is given by:

$$P_0 = \frac{c^2{}_s\rho_0}{\gamma} \quad (8)$$

with c_s the speed of sound at the reference density and γ is a problem dependent parameter.

Thermal Energy

The rate of thermal energy, associated to each particle, is calculated using the expression given by Cleary [30]:

$$\frac{dE_a}{dt} = \sum_b \frac{4m_b}{\rho_a\rho_b}\frac{k_a k_b}{k_a + k_b}T_{ab}\frac{r_{ab}.\nabla_a W_{ab}}{r_{ab}^2 + \varepsilon^2} \quad (9)$$

k_a and k_b are the conductivity of particle a and b, T_{ab} is the difference between the temperatures of particles a and b. This equation involves an explicit conductivity which can be variable. This allows to accurately simulate heat transfer of multiple materials with different conductivities.

BOUNDARY CONDITIONS

Mold Representation

One of the problems of the SPH method is the particle deficiency near or on the boundary. For particles near or on the boundary, only particles inside the boundary contribute to the particle interaction, and any contribution comes from outside because there are no particles beyond the boundary. Some improvements have been proposed to treat the boundary condition; there are mainly three types of particles to model boundaries: the ghost particles [31], the repulsive particles [19], and the mirror particles [21].

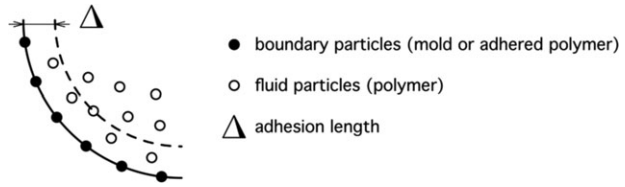

FIG. 2. Adhesion scheme.

In our simulations, we implemented the repulsive boundary and the mold is represented by one layer of solid particles. It rotates around one or two perpendicular axes according to the configuration (2D or 3D). To avoid fluid particles penetrating over solid boundaries, a force is applied between a solid particle and a neighboring fluid particle. A type of Lennard–Jones force is used as the repulsive force [19], PB_{ab}:

$$PB_{ab} = \begin{cases} D\left[\left(\frac{r_0}{r_{ab}}\right)^{n_1} - \left(\frac{r_0}{r_{ab}}\right)^{n_2}\right]\frac{x_{ab}}{r_{ab}^2} & \left(\frac{r_0}{r_{ab}}\right) \leqslant 1 \\ 0 & \left(\frac{r_0}{r_{ab}}\right) > 1 \end{cases}. \quad (10)$$

Parameters $n1$ and $n2$ are usually taken as 12 and 4, respectively, D should be chosen to be in the same scale as the square of the largest velocity and r_0 is the distance from which the fluid particles interact with the solid particles.

Adhesion of Particles

Usually, boundary conditions developed for SPH method prevent penetration and produce no-slip conditions. In this configuration, fluid particles cannot adhere to the boundary particles (except for very low velocities). To simulate the adhesion of the reactive fluid on the mold surface, we developed a model to fix the fluid particles when they reached a certain viscosity and when they are exposed to a certain distance from the mold (or the fixed material) during a certain time. Figure 2 shows a schematic representation of the fluid particles and the boundary particles (mold or adhered polymer). The adhesion length is the distance from the boundary from which the fluid particles can adhere. To fix a fluid particle, three criteria must be verified:

- The effective particle viscosity η_a must be higher than the adhesion viscosity, η_{adhe} (viscosity from which the polymer starts to adhere on the mold surface).
- The distance of the fluid particle and the boundary r_{ab} must be lower than the adhesion length Δ.
- The exposure time T_{expo} of a fluid particle must be higher than the adhesion time t_{adhe}. The count down is engaged when $r_{ab} \leq \Delta$.

η_{adhe} and t_{adhe} are physical parameters linked to the surface roughness and the rotation speed of the mold. They are determined by experimental measurements using a homemade device. Δ is a numerical parameter and is chosen to be in the same scale than the smoothing length. When polymer gelation occurs, the material becomes stiff and there is no more flow. The plastic part can be removed from the mold. To simulate gelation phenomena, the remaining fluid particles must be fixed. When the fluid particles viscosities η_a reach a viscosity close to the gel point η_{gel}, they become fixed, even if they do not satisfied the three above mentioned criteria. At this step, the simulation process is completed.

IMPLEMENTATION

Neighbors Search Algorithm

Because in SPH method the approximation of particle properties are defined by the summation over all the particles within the region of compact support of the kernel function, it is necessary to locate nearest neighbors for each particle. This task is clearly dependant of the number of particles N. The easiest method to implement is the all-pair search method which consists for a given particle to check if all the others one are within the radius of the compact support. The number of operations necessary to build the neighbors list for each particle is then N^2. When applying this method to a high number of particles, the time necessary to build the list of neighbors increases dramatically. In our code we choose to implement the linked-list search algorithm which works well in the case of a constant smoothing length [33, 34]. Here the computational time decrease considerably since $N \log N$ operations are necessary to build the list of neighbors. Basically this method consists in the use of a virtual grid over the problem domain where the sizes of the cells are of compact support order (Fig. 3). Each particle is assigned to a cell and a list of particles is created for each cell. Then for a given particle, its nearest neighboring particles can

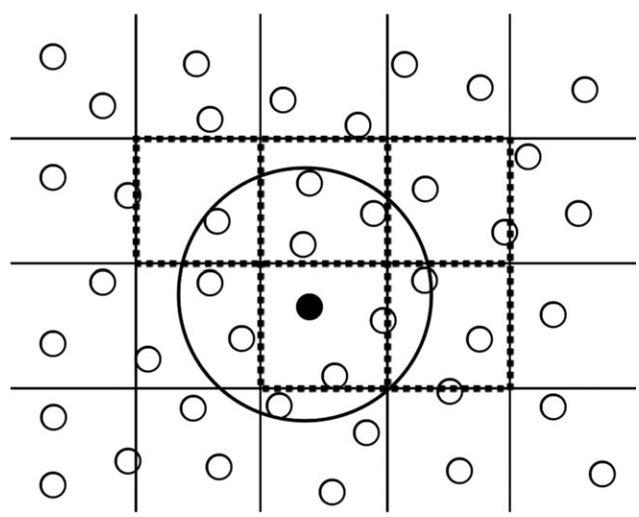

FIG. 3. In 2D configuration, the domain is divided in square cells of side $2h$. To find the neighbors of the black particle within the compact support, only the dotted cells need to be checked.

only be in the same grid cell or in the neighboring cells. To improve the algorithm it is also possible to use the symmetry of the particle interactions. Then if the search is carried out for grid in ascending numerical order, it is not necessary to check the particles in a cell labeled with a lower number (Fig. 3). This reduces the grid to be check at 5 in 2D and 13 in 3D.

Time Stepping

The numerical scheme used is the explicit Newmark algorithm [35]. The variables are calculated according to:

$$v_i^{n+1} = v_i^n + \Delta t\left((1-\alpha)a_i^n + \alpha a_i^{n+1}\right) \tag{11}$$

$$x_i^{n+1} = x_i^n + \Delta t v_i^n + \Delta t^2\left((0.5-\beta)a_i^n + \beta a_i^{n+1}\right) \tag{12}$$

with x the position and v the velocity. Moreover $\alpha = 0.5$ and $\beta = 0.25$. The temperature and the density are updated according to (11) and the time step Δt depends on the Courant Friedrichs Lewy condition [23]. The Newmark algorithm is a second-order scheme.

Parallel Computing

To enhance the performance of the code on multicore computers we used the OpenMP® application for the most time consuming parts of the solver (neighbors list construction and computation force).

VALIDATION

Couette Flow

The first test case used to validate this SPH algorithm is the 2D Couette flow [21]. The incompressible fluid is located between two infinite plates. The system is initially at rest and when simulation starts the upper plate moves at constant velocity V_0 parallel to the x-axis. The gap between the two plates is $y = L$. The analytical values are given by the following equation:

$$V_x(y,t) = \frac{V_0}{L}y + \sum_{n=1}^{\infty}\frac{2V_0}{n\pi}(-1)^n \sin\left(\frac{n\pi}{L}y\right)\exp\left(-\nu\frac{n^2\pi^2}{L^2}t\right) \tag{13}$$

where V_x is the fluid velocity in the x-direction. The kinematic viscosity $\nu = 10^{-6}$ m^{2}s^{-1}, $L = 10^{-3}$ m, $\rho = 10^3$ kg m^{-3} and $V_0 = 1.25 \times 10^{-5}$ m s^{-1}. This corresponds to a Reynolds number of 1.25×10^{-2}, using:

$$R_e = \frac{V_0 L}{\nu} \tag{14}$$

Figure 4 shows the comparison of the SPH simulation results and the analytical solution for the Couette flow. These results are in close agreement, confirming the accuracy of the SPH algorithm to evaluate low Re incompressible flows.

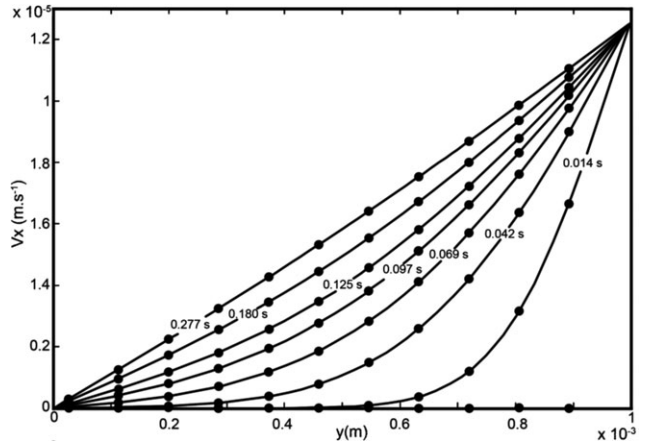

FIG. 4. Couette flow: comparison between the SPH results (●) and the analytical solution (—).

Dam Break

We performed a second test case to validate this SPH solver. The broken dam problem is a classical problem involving free surfaces and rapid motion [35, 36]. Even if this test seems far from the field of rotational molding, it is a good way to test the repulsive boundary condition and the free surface representation. The problem consists of a rectangular column of fluid confined between a fixed wall and a temporary wall (dam). At time $t = 0$, the dam is removed allowing the fluid column to collapse under the influence of gravity. Martin and Moyce [37] obtained the experimental data for the collapse of a water column. In this simulation, the problem is represented by approximately 4000 particles and the fluid viscosity is set at 0.001 Pa s (water at 20°C). Figure 5 shows the collapse of the water column at various times. The comparison between the experimental measurements and the simulation results are given in Fig. 6, the nondimensional surge front positions of the collapsing dam are plotted against the nondimensional time. As previously, the results are in good agreement, the developed SPH solver is then validated and we can now apply this algorithm to simulate RRM.

APPLICATION TO RRM

Currently, there is no test case to validate simulation of polymer flow during RRM. Thus we developped a test case destined to become a standard. The test should be simple with a known final solution. It should be experimentaly feasible to be able to compare the simulation with the experiment. Finally it must validate the simulation parameters and particularly the boundary condition of the artificial adhesion. The test is discribed in the next section.

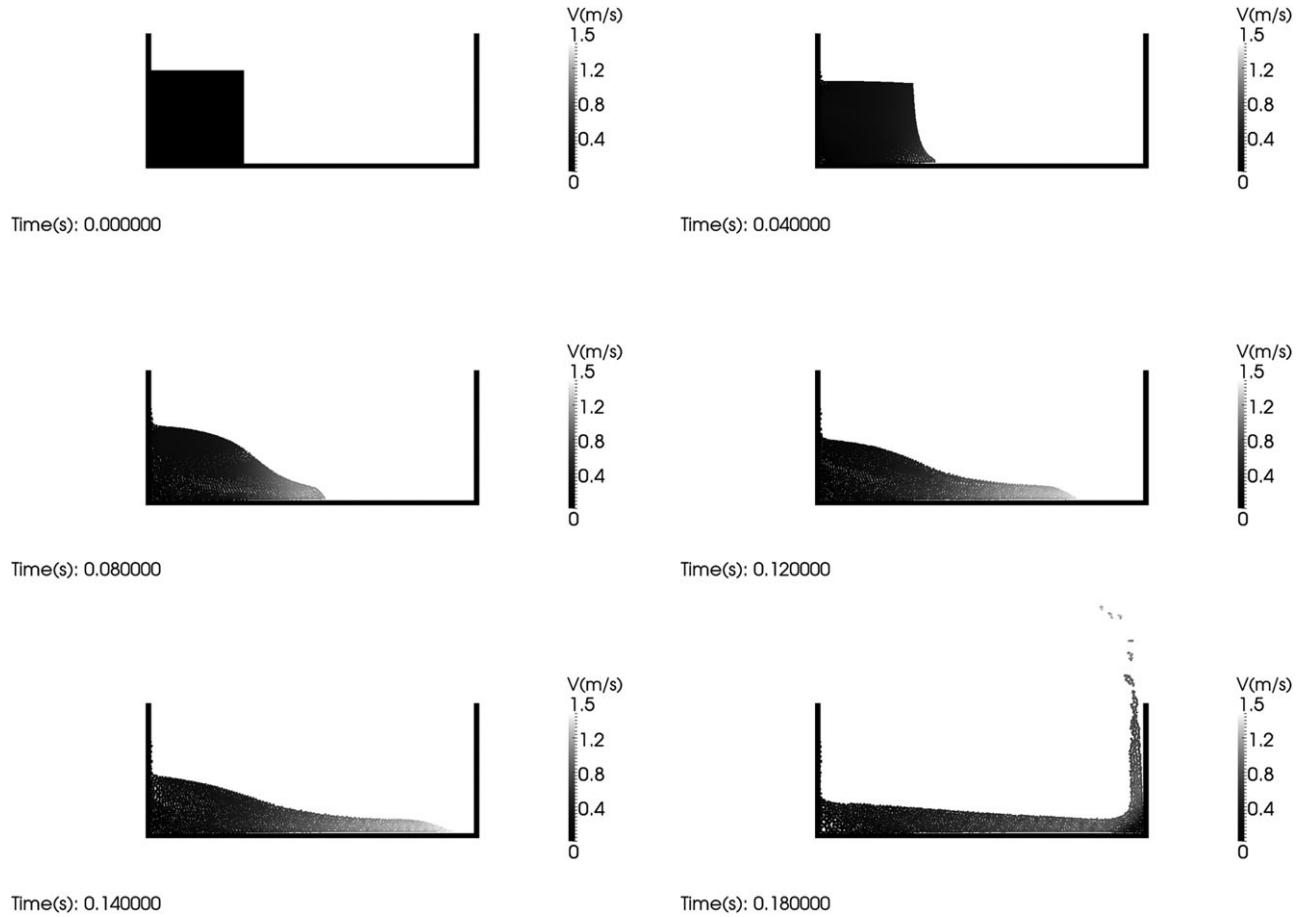

FIG. 5. Collapse of a water column.

Simulation and Validation in 2D

We performed 2D simulations of an increasing viscosity fluid in a mold. To test the efficiency of the adhesion model, we used a simple geometry consisting in a cylinder rotating around its main axis. The cylinder radius is 8 cm and the rotational speed is 7 rpm. The initial interparticle distance dx is 4.2 x 10^{-4} m. The mold is represented of approximately 1000 solid particles and its temperature is set at 60°C. The polymer which is a polyurethane has a density of 1200 kg m^{-3} and is symbolized of approximately 19,000 fluid particles. The initial fluid temperature is set at 25°C. A rheokinetical model [26] is implemented for this material to simulate the variation of viscosity according to the conversion ratio and the temperature. With the initial amount of polymer, the final part wall thickness should be approximately of 4 mm. At the end of the simulation, around 10 particles should form the part wall thickness. While writing this article, the experimental device allowing the determination of η_{adhe} and t_{adhe} for the adhesion model is still on development. Then we decided to introduce in the model, the values that we thought close to the reality. η_{adhe} is of the scale of a few Pascal seconds and t_{adhe} of few seconds. t_{adhe} decreases with time to take into account the effect of increase in the viscosity on adhesion speed. Consequently, the polymer layers on the mold surface are formed more rapidly with time increasing according to reaction rate. The computational time is rather important, and then we started the simulation for a fluid viscosity higher than η_{adhe}. At this step the polymer can start to adhere on the mold surface. Figure 7 shows the results for this 2D simulation. First of all, we can see that the reactive material is well

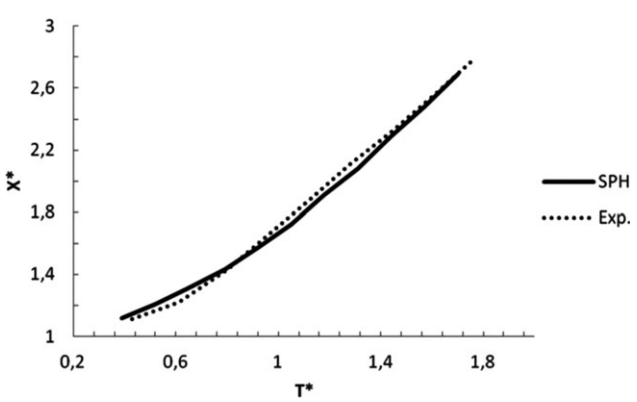

FIG. 6. Surge front for experiment (●●●) and SPH simulation (—). Nondimensional maximum x-position $X^* = X/a$ versus nondimensional time $T^* = t(g/a)1/2$ (a is the initial column width).

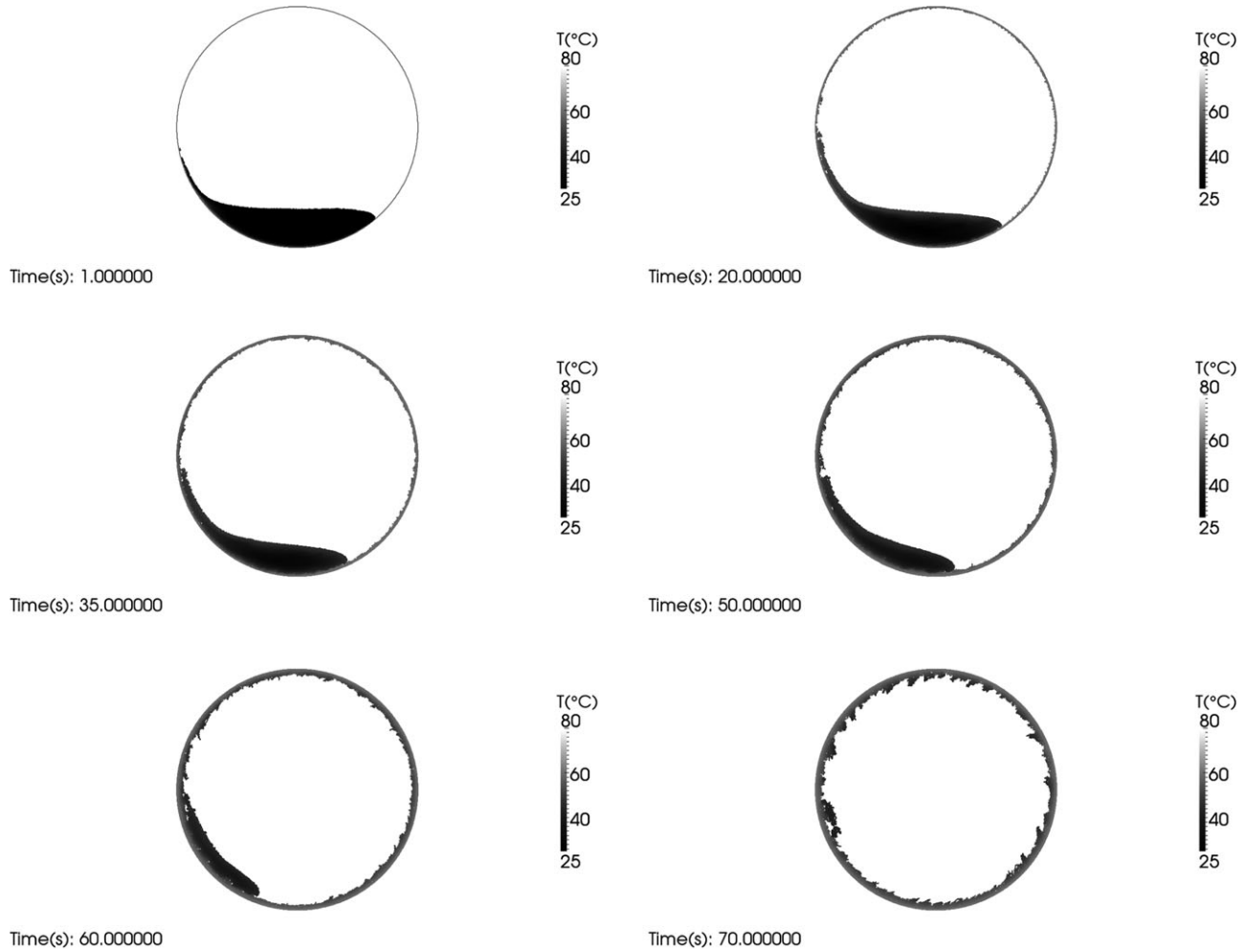

FIG. 7. 2D cylinder (20,000 particles).

represented thanks to a high number of particles (20,000). Since $\eta_a > \eta_{\text{adhe}}$, the reactive material starts to adhere at the early steps of the simulation. t_{adhe} is high (approximately 3 s) then the fluid particles adhere slowly to the mold surface. After 20 s, we can observe a thin layer of polymer on the mold surface represented by one or two particles. In the same time, heat transfer between the mold and the reactive material is well represented; the adhered particles are at the mold temperature whereas the fluid particles in the middle of the polymer are still at 25°C. From this range of viscosities we can observe the cascading flow described in Fig. 1, the material adhere to the mold but due to the gravity it falls down. From 50 s, t_{adhe} starts to decrease significantly and combined to increase in the viscosity, fluid particles can quickly adhere on the mold surface. A polymer layer is formed of several particles (3 or 4). Between 50 and 70 s, we can observe the rimming flow. The material is well distributed on the mold surface and the plastic part starts to appear, but remaining fluid particles create a wave phenomenon on the fluid surface. After 70 s the solid rotation occurs, the polymer is relatively well distributed on the mold, η_a is close to η_{gel}, at these viscosities the fluid particles stick to the fixed polymer layer. The final part dimensions are almost set and the thickness is approximately of 10 particles. Once η_{gel} reached ($\eta_{\text{gel}} = 1500$ Pa s), the part becomes stiff and there is no more flow, the simulation stops. Even if the parameters of the adhesion model were not defined by experimental measurements, we could observe the main flows described in Fig. 1 and the capability of the developed method was demonstrated for the 2D configuration. Improvements must be added notably to avoid the creation of particle clusters as we can see on the final part (70 s). A better estimation of the adhesion model parameters and an increase in the particles number necessary to model the fluid, could reduce this phenomenon.

Simulation Results in 3D

As previously for the 2D configuration, to test the adhesion model we started the 3D simulation with a simple mold geometry. We modeled a cylindrical shape of 20 cm length and of 10 cm diameter. The initial interparticle distance dx is set at 2.5×10^{-3} m. The mold is represented of approximately 12,000 solid particles and it rotates

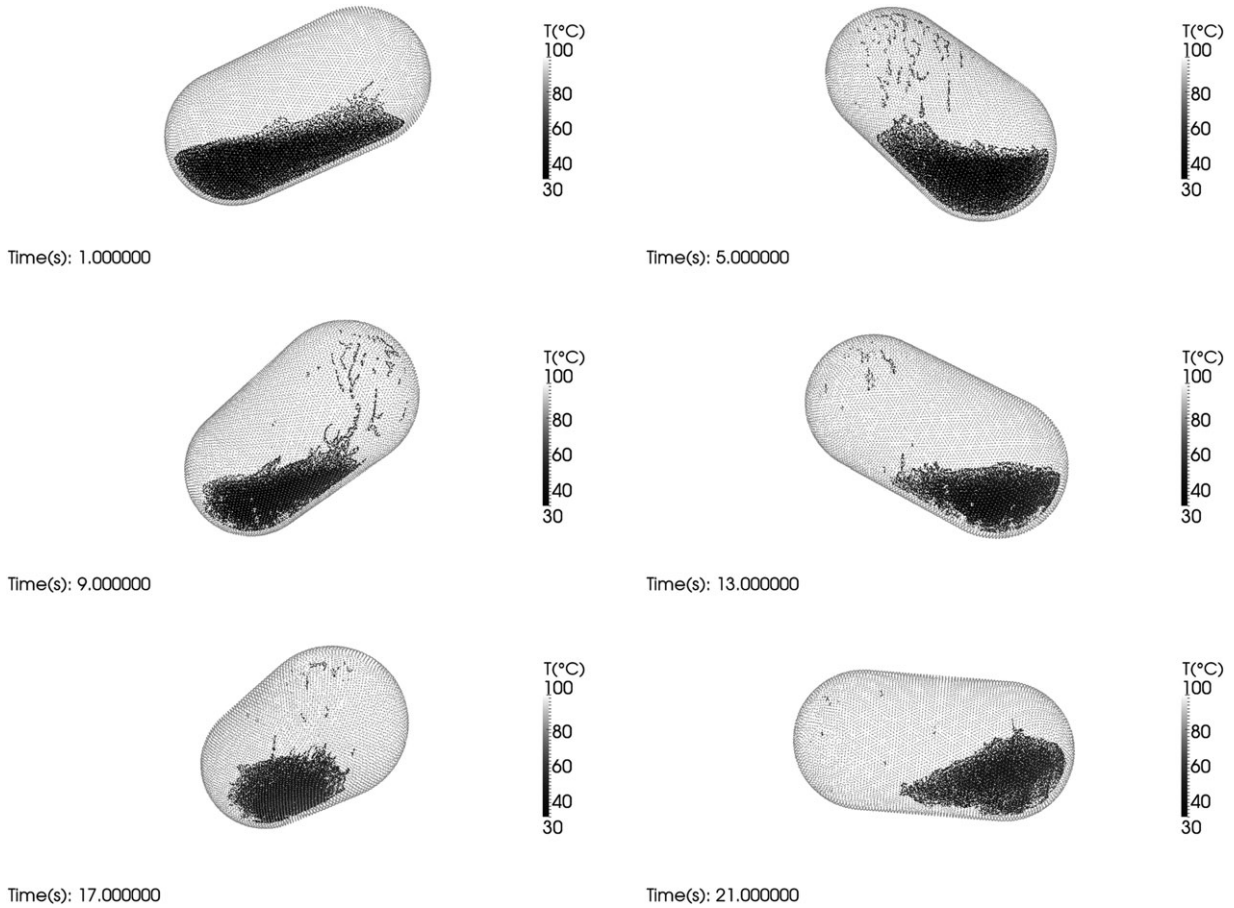

FIG. 8. 3D cylinder (35,000 particles).

according two perpendicular axes with two different velocities: 5 and 7 rpm. The mold temperature was set at 80°C. The reactive fluid is symbolized of approximately 23,000 fluid particles. Like the 2D configuration, the evolution of viscosity of the polyurethane is simulated by a rheokinetical model. The volume of polymer introduced in the mold corresponds to a final part of 4 mm thickness. Since dx is 2.5×10^{-3} m, the final thickness is only represented of one or two particles, this is very little. If we

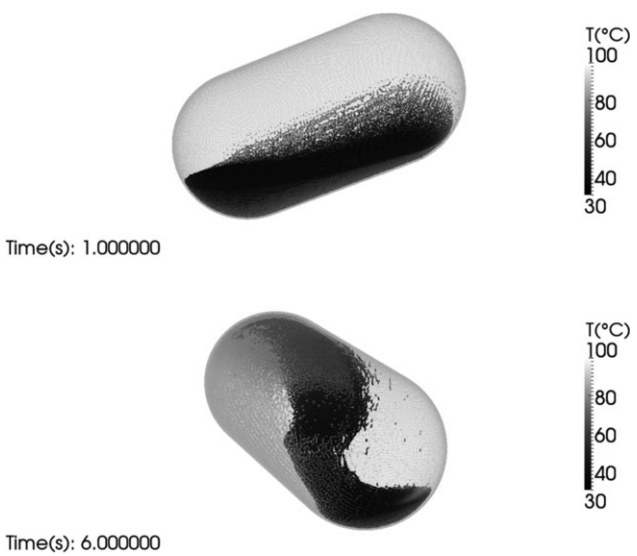

FIG. 9. 3D cylinder (400,000 particles).

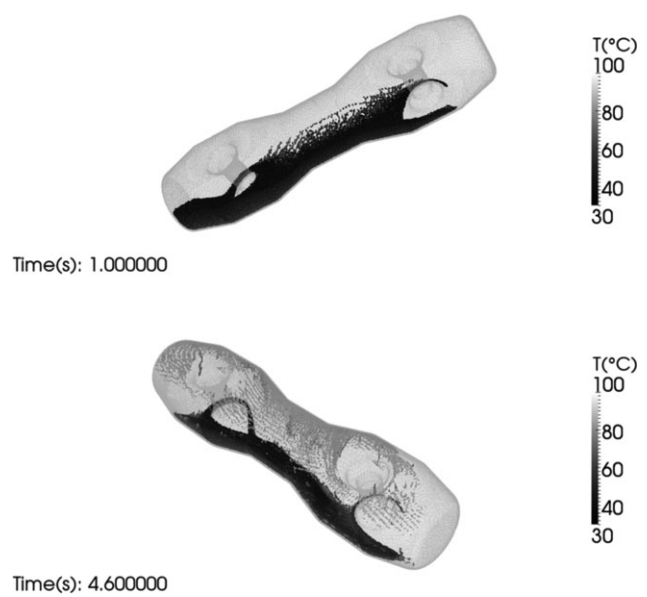

FIG. 10. Liner (260,000 particles).

used the previous parameters for the model of adhesion, in this configuration all the material would have adhered in a half rotation. To avoid this, we increased t_{adhe}. Figure 8 shows the simulation results for this 3D cylinder. The flow is well represented but heat transfer is too fast because the fluid resolution is too low (small number of particles). Only few particles can adhere and they formed some lines. The material is not well distributed on the mold surface. These results could be explained by the lack of particles to model the fluid. We did the same simulation but we changed dx from 2.5 to 1 mm and we set t_{adhe} as the 2D configuration. Now the mold with the reactive polymer is represented by 400,000 particles. In Fig. 9, we can see that the polymer flow is more realistic, such as heat transfer. Adhesion of particles is better than previously, we can observe the formation of a homogeneous layer. The model seems to work for 3D simulations too. However, the final thickness should be represented of four particles which is still a low resolution. To be able to simulate a realistic 3D flow with an accurate adhesion process, few millions of particles are necessary. Currently, we can only perform simulations of few hundred thousands of particles, it takes already a long computational time (days). To simulate millions of particles, the solver should be parallelized on a graphical processing unit (GPU). The simulation speed achieved should be of one or two orders of magnitude faster than the equivalent central processing unit code [38]. Finally we also simulated RRM for an industrial part. Figure 10 represents the inner part of a pressurized gas tank (liner). The dimensions of the part are approximately of 80 cm length and 20 cm diameter. 260,000 particles are used to model the mold and the fluid ($dx = 2.5 \times 10^{-2}$ m). The same remarks can be made than the previous 3D cylinder case.

CONCLUSIONS

Simulating the polymer flow during RRM is of great interest to optimize the process parameters and the design of the molds. We developed a solver using the SPH method and several test cases were performed to validate the code. Adhesion of the polymer on the mold surface was modeled by a new boundary condition. The obtained results are encouraging particularly for the 2D configuration. We could simulate the main hydrodynamic regimes occurring during RRM until the gel point of the reactive material. At the end of the simulation process, the material was well distributed on the mold surface. For 3D simulations, the results were less satisfying mainly because a high number of particles are needed to simulate realistic flows. Improvements of the adhesion model are still necessary, notably the determination of the parameters and the way the fixed particles interact with the fluid particles to avoid clusters formation. Moreover the parallelization of the solver on GPU could allow the simulation of millions of particles to predict realistic 3D flows in complex mold geometries. A next study will be focused on a parametric analysis to clearly identify the influence and the limits of the adhesion model parameters. The development of the experimental device will help us to determine the best parameters to be introduced into the model.

REFERENCES

1. R.J. Crawford and J.L. Throne, *Rotational Molding Technology, Plastics Design Library*, John Wiley & Sons Inc., New York (1996).
2. A. Tcharkhtchi, Rotomoulage de pièces en matière thermoplastique, Techniques de l'Ingénieur, AM 3706 (2004).
3. J.L. Throne and J. Gianchandani, *Polym. Eng. Sci.*, **20**, 13 (1980).
4. E. Harkin-Jones and R.J. Crawford, *Polym. Eng. Sci.*, **36**, 5 (1996).
5. E. Mounif, V. Bellenger, P. Mazabraud, F. Nony, and A. Tcharkhtchi, *J. Appl. Polym. Sci.*, **116**, 2 (2010).
6. J. Viale, F. Nony, P. Mazabraud, J-F. Gérard, A. Tcharkhtchi, and G. Doulin, *Int. J. Mater. Form.*, **1**, 1 (2008).
7. S. Farzaneh, S. Riviere, and A. Tcharkhtchi, *J. Appl. Polym. Sci.*, **125**, 2 (2012).
8. N. Barhoumi, K. Lamnawar, and A. Maazouz, *Int. J. Mater. Form.*, **1**, 1 (2008).
9. E. Mounif, G.G. Liang, W.D. Cook, V. Bellenger, and A. Tcharkhtchi, *Polym. Int.*, **58**, 8 (2009).
10. J.B. Enns and J.K. Gillham, *J. Appl. Polym. Sci.*, **28**, 8 (1983).
11. J.K. Gillham, *Polym. Eng. Sci.*, **26**, 20 (1986).
12. E. Mounif, V. Bellenger, and A. Tcharkhtchi, *J. Appl. Polym. Sci.*, **108**, 5 (2008).
13. A. Tcharkhtchi, S. Khelladi, and R. Rey, *Rotation*, **13**, 1 (2004).
14. E. Mounif, Résines époxy/amine pour le rotomoulage réactif: étude de la rhéocinétique et simulation numérique de l'écoulement. PhD Thesis, Arts et Métiers ParisTech (2008).
15. M.B. Roller, *Polym. Eng. Sci.*, **26**, 6 (1986).
16. P.J. Halley and M.E. Mackay, *Polym. Eng. Sci.*, **36**, 5 (1996).
17. L.B. Lucy, *Astron. J.*, **82**, 12 (1977).
18. R.A. Gingold and J.J. Monaghan, *Mon. Not. R. Astron. Soc.*, **181**, 375 (1977).
19. J.J. Monaghan, *J. Comput. Phys.*, **110**, 2 (1994).
20. J.J. Monaghan and A. Kochryan, *Comput. Phys. Commun.*, **87**, 1 (1995).
21. J.P. Morris, P.J. Fox, and Y. Zhu, *J. Comput. Phys.*, **136**, 1 (1997).
22. J.J. Monaghan, *Mon. Not. R. Astron. Soc.*, **365**, 1 (2006).
23. P. Cleary, J. Ha, V. Halguine, and T. Nguyen, *Appl. Math. Model.*, **26**, 2 (2002).
24. P.W. Cleary, *Appl. Math. Model.*, **34**, 7 (2010).
25. X.-J. Fan, R.I. Tanner, and R. Zheng, *J. Non-Newtonian Fluid Mech.*, **165**, 5 (2010).
26. F. Dimier, N. Sbirrazzuoli, B. Vergnes, and M. Vincent, *Polym. Eng. Sci.*, **44**, 3 (2004).

27. J.J Monaghan, *Annu. Rev. Astron. Astrophys.*, **30**, 543 (1992).
28. J.J Monaghan, *Rep. Prog. Phys.*, **68**, 8 (2005).
29. G.R. Liu and M.B. Liu, *Smoothed Particle Hydrodynamics A Meshfree Particle Method*, World Scientific Publishing Co. Pte. Ltd., Singapore (2003).
30. P.W. Cleary, *Appl. Math. Model.*, **22**, 12 (1998).
31. P.W. Randles and L.D. Libersky, *Comput. Methods Appl. Mech. Eng.*, **139**, 1 (1996).
32. A.J.C. Crespo, M. Gomez-Gesteira, and R.A. Dalrymple, *Comput. Mater. Con.*, **5**, 3 (2007).
33. R.W. Hockney and J.W. Eastwood, *Computer Simulation Using Particles*, Institute of Physics Publishing, Bristol (1988).
34. J.C. Simpson, *Astrophys. J.*, **448**, 822 (1995).
35. R. Ata and A. Soulaimani, *Int. J. Numer. Methods Fluids*, **47**, 2 (2005).
36. D. Violeau and R. Issa, *Int. J. Numer. Methods Fluids*, **53**, 2 (2007).
37. J.C. Martin and W.J. Moyce, *Phil. Trans. R. Soc. Lond. A*, **224**, 882 (1952).
38. A. Hérault, G. Bilotta, and R.A. Dalrymple, *J. Hydraul. Res.*, **48**,Extra Issue (2010).